

Efficient Image Deblurring Networks based on Diffusion Models

Kang Chen Yuanjie Liu*

College of Information and Electrical Engineering, China Agricultural University

Abstract

This article introduces a sliding window model for defocus deblurring that achieves the best performance to date with extremely low memory usage. Named Swintormer, the method utilizes a diffusion model to generate latent prior features that assist in restoring more detailed images. It also extends the sliding window strategy to specialized Transformer blocks for efficient inference. Additionally, we have further optimized Multiply-Accumulate operations (Macs). Compared to the currently top-performing GRL method, our Swintormer model drastically reduces computational complexity from 140.35 GMacs to 8.02 GMacs, while also improving the Signal-to-Noise Ratio (SNR) for defocus deblurring from 27.04 dB to 27.07 dB. This new method allows for the processing of higher resolution images on devices with limited memory, significantly expanding potential application scenarios. The article concludes with an ablation study that provides an in-depth analysis of the impact of each network module on final performance. The source code and model will be available at the following website: <https://github.com/bnm6900030/swintormer>.

1. Introduction

Image deblurring is a classic task in low-level computer vision, which aims to restore the image from a degraded input and has a wide range of application scenarios. Existing networks based on supervised deep learning methods such as Restormer [68], GRL [65] show strong capabilities for image deblurring tasks. However, these supervised learning algorithms require a large amount of labeled data for training. Data annotation is laborious and usually requires domain knowledge, which has led to high cost. In some tasks, obtaining large-scale annotated data is difficult or even impossible. Another important issue is the generalization ability. The current deblurring algorithms often suffer severe performance degradation when faced with data distributions different from the training data. This limitation in the model’s generalization ability can lead to a de-

Table 1. The results of defocus deblurring on the Canon DP dataset DPDD [1]. The Multiply-Accumulate operations is estimated when the input is 256×256 . Our method outperforms existing baselines, achieving state-of-the-art quality while being computationally efficient.

Method	Params (M)	MACs (G)	PSNR (dB)
DPDNet	34.52	1.88	25.13
KPAC	1.58	0.35	24.85
IFAN	14.48	0.86	25.99
Uformer	50.88	3.07	25.65
Restormer	26.13	18.70	26.66
GRL	75.57	140.35	27.04
Swintormer(ours)	154.89	8.02	27.07

cline in performance. The insufficiency of the generalization severely hindered the actual application. To address these challenges, a potentially effective approach is to employ pretrained large models to aid in supervised image deblurring tasks. Large models have seen significant advancements in recent years, with Artificial Intelligence Generated Content (AIGC) showcasing the boundless potential of AI in the future. In recent years, unsupervised learning methods have developed rapidly, such as Artificial Intelligence Generated Content (AIGC) allows people to see the infinite potential of AI in the future. The images produced by Stylegan [26], Stable Diffusion [48] and other unsupervised generation methods are amazing in their fidelity. We believe that these new models can play a powerful role in image restoration due to their outstanding advantages.

Latent image prior information Diffusion models (DM) [23], which contain billions of parameters, have shown to achieve impressive results in image synthesis, class-conditional image synthesis and super-resolution. By heavily exploiting parameter sharing, they can model highly complex distributions of natural images. In the existing supervised tasks, most of the image datasets contain only a few hundred images, and the image information is very limited. Therefore, we can use DM to learn complex distributions in the real world from large datasets such as ImageNet, CIFAR, and COCO, then sample additional information based on existing labeled datasets. This approach allows us to generate new images that possess similar characteristics with the training data, effectively expanding the size and diversity of available image datasets. Specifically,

*Corresponding author.

we intentionally optimized a latent diffusion model trained on ImageNet, fine-tuned it with dedicated datasets, and then used this model to guide the generation of image feature maps.

Mixed attention mechanism Attention mechanisms based on CNNs have proven to be effective in learning generalizable patterns from large-scale data, making them a preferred choice over traditional deblurring methods. The basic operation of ‘convolution’ in CNNs provides local connectivity and translation equivariance. Although the convolution operation enhances efficiency and generalization in CNNs, it presents two primary challenges. **(a)** The convolution operator’s receptive field is limited, hindering its ability to model long-range pixel dependencies. **(b)** The convolution filters maintain static weights during inference, limiting their flexibility to adapt to input content. As a result, algorithms utilizing the self-attention (SA) mechanism [60, 63, 69, 17] were introduced to address the aforementioned issues. Although SA is highly effective in capturing long-range pixel interactions, its complexity grows quadratically with the spatial resolution. This makes it impractical to apply to high resolution images, which is often the case in image deblurring. Recently, there have been some attempts to customize the attention mechanism for image deblurring tasks [34, 64, 68]. To reduce the computational loads, these methods either apply SA on small 8×8 spatial windows around each pixel [34, 64, 65], or substitute the fully connected layer in the attention mechanism with a more efficient sparse convolution operation [68]. Both methods offer distinct advantages, thus we propose an efficient mixed Transformer for image deblurring that delivers improved performance through spatial attention and channel attention.

In this paper, we propose a novel approach for image deblurring that is capable of fusing more image information and also applicable for large images. Firstly, we use a DM model that loads the best pre-trained parameters to generate latent image features based on existing supervised dataset. We then proceed to train the deblurring network by inputting the latent image features and the label dataset simultaneously. Lastly, we present a broader approach to addressing the inconsistency in the distribution of global information during training and inference. The main contributions of this work are summarized below:

- We propose Swintormer, a Sliding Window Transformer for multi-scale representation learning on high-resolution images. It incorporates latent image feature fusion to effectively deblur images.
- We propose a novel training scheme that utilizes DM to generate image features conditionally, enabling the model to learn additional prior information.

- We propose a more efficient method for attention computation in image processing, which includes both channel attention and spatial attention. The channel attention is a multi-Dconv head transposed attention and the spatial attention is a shifted windows-Dconv attention (SWDA).
- We present a more general approach by dividing the image into overlapping patches for independent inference, which improves the model performance.

2. Related Works

2.1. Image deblurring

Currently, the work on image deblurring using deep learning involves establishing a direct mapping between blurred images and sharp images from paired datasets:

$$I_b = \phi(I_s; \theta_i), \quad (1)$$

where ϕ is the image blur function, and θ_i is a parameter vector. I_s is the sharp image. I_b is the blurred image. With the powerful fitting capability of deep learning, it is possible to directly train the model end-to-end to learn this mapping, thereby achieving deblurring [64, 65, 68]. Current research primarily focuses on general algorithms that aim to improve model representation by using advanced neural network architecture designs such as residual blocks, dense blocks, attention blocks, and others [61, 38, 36, 37, 22, 8, 15, 20, 28, 19]. Table.[tab:benchmark] compares the computational complexity with common methods.

Another approach involves developing specific models that optimize network structures based on the given task, including classical/lightweight image SR, real-world image SR, color/grayscale image denoising and JPEG compression artifact reduction [21, 70, 34, 7].

2.2. Vision Transformer

The Transformer model [60] was initially proposed for sequence processing in natural language tasks. Subsequently, its robust adaptability led to the development of the Vision Transformer (ViT) [17] for image processing. To balance speed and accuracy, the ViT applies a Transformer architecture on non-overlapping medium-sized image patches and learn their mutual relationships. While there are other models that excel in theory and interpretability than Transformer, none surpass its performance. As a result, researchers are focusing on understanding the factors that contribute to the Transformer’s success. Numerous experiments indicate that the effectiveness of the Transformer primarily lies in the design of token mixer and the FFN(Feed-Forward Network) [66]. In particular, the self-attention mechanism in the token mixer is recognized as the key driver of its superior performance. However,

Layer Type	Per-layer Complexity	Sequential Operations	Maximum Path Length
Self-Attention Layer	$O(T^2 \cdot D)$	$O(1)$	$O(1)$
Dense Layer	$O(T^2 \cdot D^2)$	$O(1)$	$O(1)$
convolutional Layer	$O(k \cdot T^2 \cdot D^2)$	$O(1)$	$O(\log_k(T))$
Recurrent Layer	$O(T \cdot D^2)$	$O(T)$	$O(T)$

Table 2. Per-layer computational complexity of common layers in neural networks.

its complexity increases quadratically as the number of patches grows, making it infeasible for high-resolution images. To address this issue, many methods utilize various token mixers to reduce complexity in different image processing applications. One approach is to incorporate attention within local image regions, as seen in models like Swin Transformer and Neighborhood Attention Transformer. Another solution involves applying attention to the channel-wise dimension instead of the spatial dimension. Additionally, there are feedforward network designs such as Mlp[4], GluMlp[14], GatedMlp[39], ConvMlp[33] and SimpleGate [5]. While these designs have their own advantages and disadvantages in various low-level visual tasks, the performance difference remains consistent when the number of model parameters is nearly the same. Table.2 compares the complexity, sequential operations, and maximum path length of self -attention with common token mixer and FFN types in image deblurring.

2.3. Latent Diffusion Model

Recently, Diffusion Models have achieved state-of-the-art results in unconditional image synthesis. Previously, common models like feed-forward, GAN, and flow-based models all directly learn a mapping from inputs to results:

$$y = f(x), \quad (2)$$

The diffusion model takes a different approach by treating the generation process as an optimization process.

$$y = \arg \min_y E_\theta(x, y), \quad (3)$$

The information it directly learns is not the joint distribution of pixels, but rather the gradient of the distribution. In other words, instead of learning a map directly, DM builds a neural network to find a solution about optimization problem and then samples the solution to get image.

Leveraging its strong capability to understand the dataset, various impressive diffusion frameworks have been utilized for low-level vision tasks. For example, IR-SDE achieves highly competitive performance in quantitative comparisons on image restoration [42], DiT [46], which replaces the commonly-used U-Net backbone with a Transformer, achieves superior results in class-conditional image generation [49, 23, 55, 16]. LDM [48] employs compression encoding process of VQGAN [18] for generating high-

resolution images. However, training the most powerful diffusion model often requires expensive computing resources, and unsupervised models often perform worse than supervised models. To address this limitation, we propose to circumvent this drawback with our Swintormer approach, which involves freezing the body and encoder of the diffusion model, and solely fine-tuning the decoder in a supervised manner. This makes training computationally more affordable while achieving the same effect as the supervised model.

3. Motivation

3.1. DM’s imperceptible modeling ability

We explore DM’s subtle modeling capability by directly using Robin’s pre-trained super-resolution DM [48] to produce high-resolution images on the deblurring dataset DPDD [1]. Remarkably, even after the inevitable downsampling to match the input image size, as shown in Table 4, we observe a substantial performance enhancement of 0.24dB for single pixel defocus deblurring. This attests to DM’s proficiency in deblurring task.

DM’s ability of implicit modelling benefits from a surfeit of training data with diverse images, improving its understanding of image content and structure for detail recovery in various conditions. DM’s uses maximum likelihood estimation to find parameters best fitting the training data distribution:

$$\nabla_\theta \|\epsilon - \epsilon_\theta(z_t, t)\|_2^2. \quad (4)$$

where z is prior feature, $t \in [1, T]$ is a random time-step and $\epsilon \sim \mathcal{N}(\mathbf{0}, \mathbf{I})$ denotes sampled noise. The unique training strategy has given it a significant advantage in its ability to generalize across various conditions. However, it is not well-suited for supervised learning tasks like classification or regression, as its main focus is on modeling the data distribution rather than predicting specific target values. Consequently, we are now undertaking an exploration of fine-tuning and adjustments rooted in the DM paradigm, in a collaborative effort to improve its performance across a range of tasks.

3.2. Attention Mechanisms for Image deblurring

Previous attention mechanisms for image deblurring have utilized various innovative approaches to mitigate the time and memory complexity of the key-query dot-product

Table 3. Long-Range Arena benchmark [58]. Results have been compiled from the original paper. Benchmarks are run on 4x4 TPU V3 chips, and the memory is reported per device.

Models	Average score (%)	Steps per second		Peak memory (GB)	
		1K	4K	1K	4K
Transformer [60]	54.39	8.1	1.4	0.85	9.48
Sparse Transformer ⁰ [9]	51.24				
Longformer [3]	53.46				
BigBird [67]	55.01	7.4	1.5	0.77	2.88
Sinkhorn Transformer [57]	51.39	9.1	5.3	0.47	1.48
Reformer [30]	50.67	4.4	1.1	0.48	2.28
Linformer [62]	51.36	9.3	7.7	0.37	0.99
Synthesizer [56]	51.39	8.7	1.9	0.65	6.99
Linear Transformer [27]	50.55	9.1	7.8	0.37	1.03
Performer [11]	51.41	9.5	8.0	0.37	1.06

Model	PSNR \uparrow	SSIM \uparrow	MAE \downarrow	LPIPS \downarrow
Input	23.70	0.713	0.048	0.354
JNB [51]	23.69	0.707	0.048	0.442
EBDB [25]	23.94	0.723	0.047	0.402
DMENet [31]	23.90	0.720	0.047	0.410
Diffusion	23.94	0.727	0.047	0.349

Table 4. Quantitative comparison by applying diffusion model [48] on the DPDD Dataset [1]. In order to make a fair comparison with other existing methods, the input image is an 8-bit image instead of a 16-bit image.

interaction. Our aim is to integrate the advantages of these diverse methods in order to devise a more effective attention calculation approach.

3.3. The information inconsistency in training and inference

Many deblurring models grapple with the challenge of inconsistency between training and inference. Take Restormer[68], for example, where the training process involves a $128 \times 128 \times 3 \times 8$ tensor input, yet during inference, a $1680 \times 1120 \times 3 \times 1$ tensor is used. This discrepancy between training and inference can detrimentally affect a model’s performance. A recent approach, TLC[12], addresses this issue by substituting global operations (like global average pooling) with local operations at inference time. However, this module-swapping technique doesn’t universally apply to all models. Hence, we introduce a novel strategy to ensure consistency between the input tensor sizes used in both training and inference. This is achieved by incorporating a pre-processing operation that employs shifted windows before the inference step. While this pre-processing operation may introduce additional computational overhead as overlapping regions are redundantly processed by the entire model, it also increases parallelization due to maintaining the same batch size, thereby expediting the inference process. Moreover, this approach grants control over the size of the overlapping

region by adjusting the sliding pace, allowing for a more nuanced trade-off between deblurring quality and inference speed in practical applications. For more comprehensive insights into the inference process, please refer to Section 4.5.

4. Method

Our goal is to develop an image deblurring model based on diffusion models. To alleviate the computational bottleneck, we propose a key training strategy: freezing the backbone and the encoder, and exclusively fine-tuning the decoder under supervision. Then we introduce an efficient mixed attention mechanism that incorporates multi-Dconv head transposed attention for channel attention calculation and Shifted Windows-Dconv Attention (SWDA) for spatial attention calculation. Finally, we introduce an image deblurring model that merges the latent features extracted by the Diffusion model and can serve as a reference design for the decoder model in the diffusion model.

4.1. Overall Architecture

An overview of the pipeline is presented in figure.1. Given a blurry image $x \in \mathbb{R}^{H \times W \times 3}$ where $H \times W$ denotes the spatial dimension, the domain specific encoder encodes x into an intermediate feature $\tau_\theta(x)$. Then, the Diffusion Model is used to conditionally generate the latent prior feature z_0 . Subsequently, the latent prior feature z_0 and the blurry image x pass through pixel-unshuffle and convolution to merge and obtain non-overlapping patches $\mathbf{P} \in \mathbb{R}^{\frac{H}{2} \times \frac{H}{2} \times C}$, which are smaller in the spatial dimension but larger in the channel dimension. These patches are then fed into a 4-level Unet network, where feature downsampling and upsampling are applied using pixel-unshuffle and pixel-shuffle operations [52]. The encoder features are concatenated with the decoder features via skip connections [50] to better preserve features details. To balance the trade-off, the number of blocks in Unet at different levels gradually increases with the downsampling of latent features. To assist the recovery performance, the la-

tent features are initially downsampled into low-resolution features $\mathbf{F} \in \mathbb{R}^{\frac{H}{16} \times \frac{W}{16} \times C}$. However, the decoder process does not simply revert the feature back to $\mathbb{R}^{H \times W \times 3}$. Instead, the decoded feature remains in the shallow feature $\mathbf{F}_s \in \mathbb{R}^{\frac{H}{2} \times \frac{W}{2} \times 2C}$ and undergoes a small Transformer to enhance structural and textural details at high spatial resolution. Finally, two residual designs are applied to further refine the features and deblur image $\hat{\mathbf{I}} \in \mathbb{R}^{H \times W \times 3}$. The modules of the Transformer block in the Swintormer are presented as follows.

4.2. Shifted Windows-Dconv attention

While self-attention [60, 17] is highly effective, the time and memory complexity of the key-query dot-product interaction grows quadratically in self-attention as the input resolution increases. For example, performing a calculation on a tensor of size $8 \times 128 \times 128 \times 48$ requires 64GB of video memory. Similar to deal with long sentence problems in NLP [9, 3, 67, 57, 30, 62, 56, 27, 11], many methods [35, 68, 5] are proposed for high-resolution image. However, these methods have different performance in different low-level visual tasks. Therefore, we propose Swintormer for improving generalization performance, that has linear complexity. The key innovation is to segment the feature tensor along the channel dimension and then calculate channel attention and spatial attention separately. Another crucial aspect is the use of depth-wise convolutions to generate *query* (\mathbf{Q}), *key* (\mathbf{K}) and *value* (\mathbf{V}) projections instead of using linear layers, which can highlight the local context to accelerate model convergence.

Given a layer normalized tensor $\mathbf{Y} \in \mathbb{R}^{\hat{H} \times \hat{W} \times \hat{C}}$, our SWDA first applies a shifted window partitioning approach to divide \mathbf{Y} into $M \times M$ patches (with a default window size of 16). One challenge with this routine is that some windows may end up smaller than $M \times M$. Therefore, a cyclic-shifting toward the top-left direction method is used to solve the problem [40]. The resulting patches are then used to generate \mathbf{Q} , \mathbf{K} and \mathbf{V} projections through 1×1 convolutions to aggregate pixel-wise cross-channel context, followed by 3×3 depth-wise bias-free convolutions. As a result, the tensors \mathbf{Q} , \mathbf{K} and \mathbf{V} are all of the same size, $\mathbb{R}^{M \times M \times \hat{C}}$. These tensors are then split into two parts along the channel, each with a size of $\mathbb{R}^{M \times M \times \frac{\hat{C}}{2}}$. One part is used for channel attention calculation by MDTA [68], where their dot-product interaction produces a transposed-attention map of size $\mathbb{R}^{\frac{\hat{C}}{2} \times \frac{\hat{C}}{2}}$, while the other part is utilized for spatial attention calculation, resulting in an attention map with size of $\mathbb{R}^{M \times M}$. Overall, the process is defined as:

$$\text{Channel Attention} = \text{SoftMax}(Q_c K_c^T) V_c, \quad (5)$$

$$\text{Spatial Attention} = \text{SoftMax}(Q_s K_s^T + B) V_s, \quad (6)$$

$$\text{Attention} = W_p^{(\cdot)} \text{concat}(\text{Channel Attention}, \text{Spatial Attention}), \quad (7)$$

where $Q_c, K_c, V_c \in \mathbb{R}^{\frac{\hat{C}}{2} \times M^2}$; $Q_s, K_s, V_s \in \mathbb{R}^{M^2 \times \frac{\hat{C}}{2}}$; $B \in \mathbb{R}^{M^2 \times M^2}$ represents the relative position bias term for each head; $W_p^{(\cdot)}$ denotes the 1×1 point-wise convolution, and M^2 is the number of patches in a window. The relative position bias encodes the relative spatial configurations of visual elements.

4.3. Diffusion model

Our diffusion model is based on latent conditional denoising diffusion probabilistic models [48, 23]. It consists of a forward diffusion process $q(z_{1:T}|z_0)$ and a reverse denoising process $p_\theta(z_{0:T})$ where T is a fixed Markov Chain of length. When given an image x , we use VQGAN [18] to obtain the latent space $z = \mathcal{E}(x)$. With the latent space, we compute the forward diffusion process for training the diffusion model and calculate the reverse denoising process for generating the prior feature.

Forward diffusion process. In the forward process, we input z and gradually add Gaussian noise \mathcal{N} to it according to a variance schedule β_1, \dots, β_T :

$$q(z_{1:T}|z_0) := \prod_{t=1}^T q(z_t|z_{t-1}), \quad (8)$$

$$q(z_t|z_{t-1}) := \mathcal{N}(z_t; \sqrt{1 - \beta_t} z_{t-1}, \beta_t \mathbf{I}) \quad (9)$$

By fixing the variances β_t to constants and the reparameterization [29] $z_t(z_0, \epsilon) = \sqrt{\bar{\alpha}_t} z_0 + \sqrt{1 - \bar{\alpha}_t} \epsilon$, for $\epsilon \sim \mathcal{N}(\mathbf{0}, \mathbf{I})$, thus Eq. (9) can be rewritten as:

$$q(z_t|z_0) = \mathcal{N}(z_t; \sqrt{\bar{\alpha}_t} z_0, (1 - \bar{\alpha}_t) \mathbf{I}) \quad (10)$$

where $\alpha_t := 1 - \beta_t$ and $\bar{\alpha}_t := \prod_{i=1}^t \alpha_i$.

Specifically, we trained a denoising network ϵ_θ by predicting ϵ from z_t , which will be discussed in Sec. 4.4.

Reverse denoising process. In the reverse process $p_\theta(z_{0:T})$:

$$p_\theta(z_{0:T}) := p(z_T) \prod_{t=1}^T p_\theta(z_{t-1}|z_t), \quad (11)$$

$$p_\theta(z_{t-1}|z_t) := \mathcal{N}(z_{t-1}; \boldsymbol{\mu}_\theta(z_t, t), \boldsymbol{\Sigma}_\theta(z_t, t)) \quad (12)$$

Following previous work [23] to accelerate reverse processing by reparameterization, we generated the prior feature z_0 using KL divergence to directly compare $p_\theta(z_{0:T})$ against forward process posteriors from z_t to z_0 :

$$q(z_{t-1}|z_t, z_0) = \mathcal{N}(z_{t-1}; \tilde{\boldsymbol{\mu}}_t(z_t, z_0), \tilde{\boldsymbol{\beta}}_t \mathbf{I}), \quad (13)$$

where
$$\tilde{\boldsymbol{\mu}}_t(z_t, z_0) := \frac{\sqrt{\bar{\alpha}_{t-1}} \beta_t}{1 - \bar{\alpha}_t} z_0 + \frac{\sqrt{\bar{\alpha}_t} (1 - \bar{\alpha}_{t-1})}{1 - \bar{\alpha}_t} z_t, \quad (14)$$

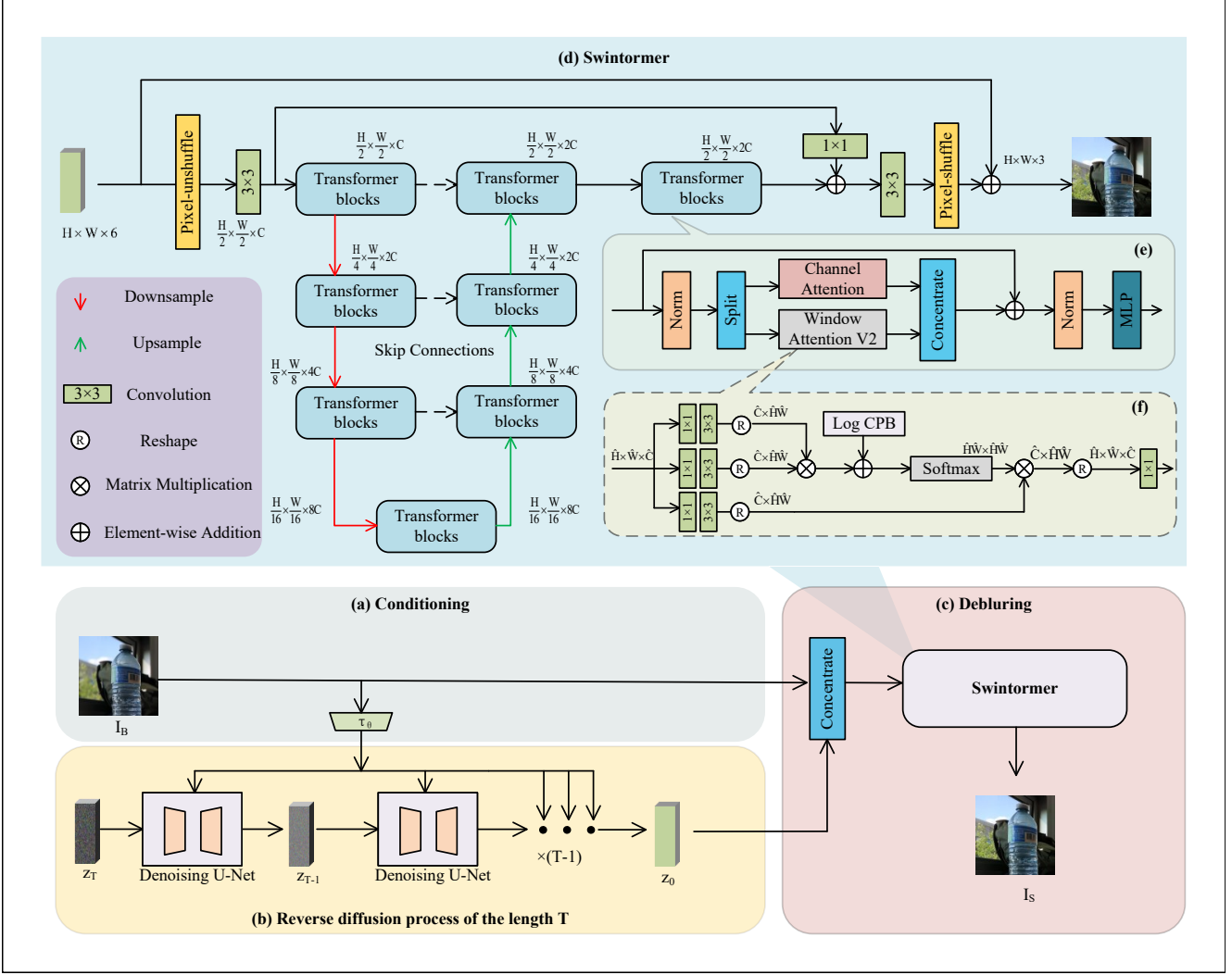


Figure 1. The architecture of the Swintormer.

$$\text{and } \tilde{\beta}_t := \frac{1 - \bar{\alpha}_{t-1}}{1 - \bar{\alpha}_t} \beta_t \quad (15)$$

Consequently, with the trained denoising network ϵ_θ conditioned on the c (The condition c could be text, semantic maps and images[24, 47, 45]) for predicting the noise ϵ , we can iteratively sample z_t as follows:

$$z_{t-1} = \frac{1}{\sqrt{\alpha_t}} \left(z_t - \frac{1 - \alpha_t}{\sqrt{1 - \bar{\alpha}_t}} \epsilon_\theta(z_t, t, c) \right) + \sqrt{1 - \alpha_t} \epsilon_t \quad (16)$$

where $\epsilon_t \sim \mathcal{N}(\mathbf{0}, \mathbf{I})$. After T iterations, we can get feature z_0 as illustrated in Fig.1(b). We further explore the iteration numbers T in Sec. 6.

4.4. Training Strategy

In our proposed architecture, there are two models needed to be trained: denoising autoencoder ϵ_θ and Swintormer. For diffusion model, we aim to generate the prior

feature based on input sample from conditional distributions of the form $p(z|c)$, so we fine-tune the latent diffusion model based on super-resolution[16], which the features generated by a super-resolution-based model are more likely to match the feature distribution of the input sample than the feature distribution of the entire dataset. As with other conditional latent diffusion models, and our fine-tune the conditional denoising autoencoder $\epsilon_\theta(z_t, t, c)$; $t = 1 \dots T$ via:

$$L_{LDM} := \mathbb{E}_{\mathcal{E}(x), y, \epsilon \sim \mathcal{N}(0,1), t} \left[\|\epsilon - \epsilon_\theta(z_t, t, \tau_\theta(y))\|_2^2 \right], \quad (17)$$

where input y is blurry image to guide the diffusion process and denoising autoencoder ϵ_θ is implemented by a time-conditional U-Net [48, 49]. Finally, we used the fine-tuned diffusion model to generate the prior feature z_0 and divide them into patches of size 256×256 . Then, we input the feature patches and origin image patches for training the

Swintormer by L_1 loss or Perceptual Loss:

$$\mathcal{L}_{deblur} = \|I_s - \phi_\theta(I_b, z_0)\|_1 \quad (18)$$

$$\mathcal{L}_{deblur} = \|VGG(I_s) - VGG(\phi_\theta(I_b, z_0))\|_2^2 \quad (19)$$

where ϕ_θ is the Swintormer model intended to deblur image and VGG is a the features extraction network[53] We will show the performance differences between these two loss functions in Sec. 5.

4.5. Inference

Upon completing the training of both the denoising autoencoder and Swintormer, given a blurry input image blurry image $x \in \mathbb{R}^{H \times W \times 3}$, the denoising autoencoder first extract the prior feature $z_0 \in \mathbb{R}^{H \times W \times 3}$. Then we concatenate them along the channel dimension to get the feature tensor $x_f \in \mathbb{R}^{H \times W \times 6}$. Before employing Swintormer for deblurring, we partition the feature tensor into the overlapping patches, resulting in the input tensor denoted as $x_{input} \in \mathbb{R}^{M \times M \times C \times B}$. Here, M signifies the window size, B is the batchsize, and the dimensions of the input tensor remain consistent with those used during training. Subsequently, the Swintormer undertakes the reconstruction of deblurred image patches $x_{dp} \in \mathbb{R}^{M \times M \times 3 \times B}$. Finally, the deblurred image patches are merged into a deblurring image $x_{db} \in \mathbb{R}^{H \times W \times 3}$ where the overlapping regions are averaged to produce the final deblurred image.

5. Experiments and Analysis

We evaluate the proposed Swintormer on benchmark datasets and experimental settings for image deblurring tasks: **(a)** defocus deblurring, **(b)** single-image motion deblurring. More details on datasets, training protocols, and additional visual results are presented in the supplementary material. In tables, the best quality scores of the evaluated methods are **highlighted**.

Implementation Details. For the latent diffusion model, we set the total time-step T as 100 and the variance hyperparameters $\beta_1 : T$ constants increasing linearly from $\beta_1 = 0.0015$ to $\beta_T = 0.0155$. Our Swintormer employs a 4-level encoder-decoder. From level-1 to level-4, the number of Transformer blocks are [4, 6, 6, 8], attention heads are [1, 2, 4, 8], and number of channels are [48, 96, 192, 384]. The refinement stage contains 4 blocks. The channel expansion factor in Feed-Forward network is $\gamma=2.66$. We train models with AdamW optimizer ($\beta_1=0.9$, $\beta_2=0.999$, weight decay $1e^{-4}$) for 300K iterations with the initial learning rate $3e^{-4}$ gradually reduced to $1e^{-6}$ with the cosine annealing [41]. The image patch size is 256×256 and batch size is 11. We use PyTorch 2.0.0, NVIDIA 2080ti GPU with CUDA11.7 to accelerate training.

5.1. Defocus Deblurring Results

Table 5 shows image fidelity scores of the conventional defocus deblurring methods. In the case of two different loss function training, our Swintormer outperforms the state-of-the-art on PSNR or LPIPS respectively. Particularly on the outdoor scene category, Swintormer yields 0.12 dB improvements over the previous best method GRL[65]. And, it is worth noting that our method achieves the highest perceptual scores in terms of LPIPS on all scene categories. Figure 2 illustrates that our method is more effective in removing defocus blur compared to other approaches.

5.2. Motion deblurring Results

Experimental results for the conventional motion deblurring are shown in Table 6. Our proposed method still maintains the advanced performance.

6. Ablation Studies

In this section, we study the effectiveness of the different designs of our proposed method. We conduct all experiments on the dataset DPDD. Table 6 show that our contributions yield quality performance improvements. Next, we describe the influence of each component individually.

Impact of diffusion prior. We construct a baseline model without prior generated from diffusion. Table 6a demonstrates that the diffusion prior provides favorable gain of 0.11dB over the baseline. Furthermore, we explore the impact of the iteration numbers T in the diffusion model. A larger number of iterations leads the diffusion model to generate more accurating features. Consequently, the later deblur model handles the features more accurating. Based on the result, when the number of iterations reaches 20, the performance improvement gradually converges. But for the better performance, we choose $T = 50$ for the final model.

Improvements in mixed attention. Table 6c shows that the shifted windows-Dconv attention has comparable performance with MDTA. Furthermore, introducing the shifted windows-Dconv attention to MDTA brings a better performance. Overall, our proposed Transformer block contributions lead to a gain of 0.08 dB over the baseline.

Improvements in pre-processing inference. Table 6b shows that pre-processing inference has comparable performance with TLC [13]. Furthermore, it’s noteworthy that without necessitating retraining or fine-tuning, a mere adjustment of the window size and shift size to align the input tensor size with the training tensor size has yielded a substantial performance improvement of 0.25 dB over the baseline.

7. Conclusions and Outlook

In this paper, we have introduced an innovative approach by integrating the DM (Diffusion Model) into tra-

Table 5. Quantitative comparison with previous defocus deblurring methods in dataset DPDD(containing 37 indoor and 39 outdoor scenes). Swintormer sets new state-of-the-art in metric PSNR and LPIPS by using the L_1 loss function and the Perceptual loss function respectively. **S**: single-image defocus deblurring. **D**: dual-pixel defocus deblurring.

Method	Indoor Scenes				Outdoor Scenes				Combined			
	PSNR \uparrow	SSIM \uparrow	MAE \downarrow	LPIPS \downarrow	PSNR \uparrow	SSIM \uparrow	MAE \downarrow	LPIPS \downarrow	PSNR \uparrow	SSIM \uparrow	MAE \downarrow	LPIPS \downarrow
EBDB _S [25]	25.77	0.772	0.040	0.297	21.25	0.599	0.058	0.373	23.45	0.683	0.049	0.336
DMENet _S [31]	25.50	0.788	0.038	0.298	21.43	0.644	0.063	0.397	23.41	0.714	0.051	0.349
JNB _S [51]	26.73	0.828	0.031	0.273	21.10	0.608	0.064	0.355	23.84	0.715	0.048	0.315
DPDNet _S [1]	26.54	0.816	0.031	0.239	22.25	0.682	0.056	0.313	24.34	0.747	0.044	0.277
KPAC _S [54]	27.97	0.852	0.026	0.182	22.62	0.701	0.053	0.269	25.22	0.774	0.040	0.227
IFAN _S [32]	28.11	0.861	0.026	0.179	22.76	0.720	0.052	0.254	25.37	0.789	0.039	0.217
Restormer _S [68]	28.87	0.882	0.025	0.145	23.24	0.743	0.050	0.209	25.98	0.811	0.038	0.178
GRL _S [65]	29.06	0.886	0.024	0.139	23.45	0.761	0.049	0.196	26.18	0.822	0.037	0.168
Swintormer _S -Perceptual	28.95	0.883	0.025	0.141	23.33	0.750	0.050	0.205	26.09	0.819	0.038	0.168
Swintormer _S -L1	28.99	0.884	0.025	0.142	23.51	0.769	0.042	0.209	26.18	0.823	0.034	0.176
DPDNet _D [1]	27.48	0.849	0.029	0.189	22.90	0.726	0.052	0.255	25.13	0.786	0.041	0.223
RDPD _D [2]	28.10	0.843	0.027	0.210	22.82	0.704	0.053	0.298	25.39	0.772	0.040	0.255
Uformer _D [64]	28.23	0.860	0.026	0.199	23.10	0.728	0.051	0.285	25.65	0.795	0.039	0.243
IFAN _D [32]	28.66	0.868	0.025	0.172	23.46	0.743	0.049	0.240	25.99	0.804	0.037	0.207
Restormer _D [68]	29.48	0.895	0.023	0.134	23.97	0.773	0.047	0.175	26.66	0.833	0.035	0.155
GRL _D [65]	29.83	0.903	0.022	0.114	24.39	0.795	0.045	0.150	27.04	0.847	0.034	0.133
Swintormer _D -Perceptual	29.55	0.897	0.023	0.107	24.40	0.796	0.045	0.147	26.91	0.845	0.034	0.128
Swintormer _D -L1	29.74	0.899	0.022	0.127	24.52	0.798	0.045	0.167	27.07	0.847	0.034	0.148

Table 6. Image Deblurring Results on GoPro[44].

Method	MIMO-UNet [10]	HINet [6]	MAXIM [59]	Restormer [68]	UFormer [64]	DeepRFT [43]	MPRNet-local[12]	NAFNet [5]	GRL [65]	Swintormer ours
PSNR	32.68	32.71	32.86	32.92	32.97	33.23	33.31	33.69	33.93	33.38
SSIM	0.959	0.959	0.961	0.961	0.967	0.963	0.964	0.967	0.968	0.965

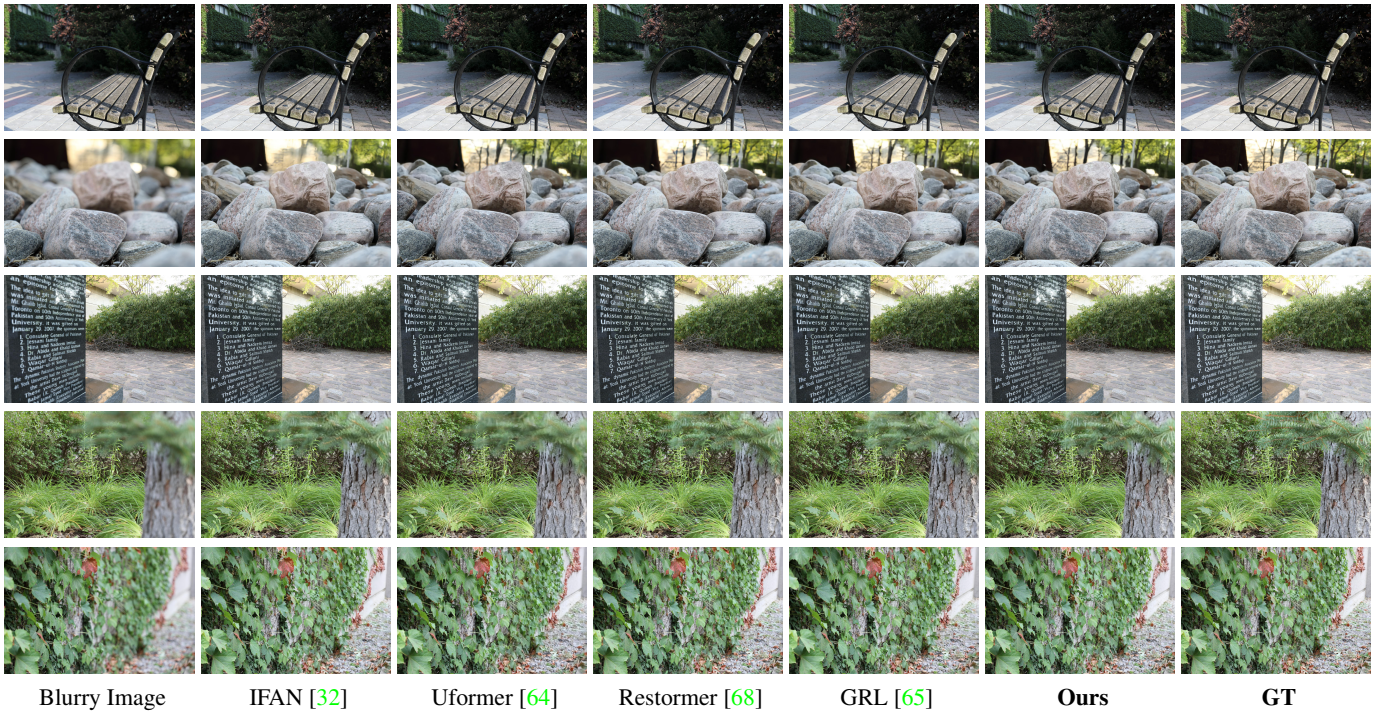


Figure 2. Dual-pixel defocus deblurring comparison on the DPDD dataset [1].

ditional image deblurring tasks. Simultaneously, we introduce Swintormer, a memory-efficient image deblurring Transformer model, designed to efficiently handle high-resolution images with remarkably low MACs (Multiply-Accumulates). Notably, our proposed Transformer block exhibits enhanced performance through the application of self-attention mechanisms that span both the channel and spatial dimensions, all while maintaining linear complexity. Furthermore, we present a plug and play methodology that

ensures consistency between the input tensor sizes during both training and inference, thereby enhancing model performance. Importantly, this approach obviates the need for retraining or fine-tuning, resulting in performance enhancements across various tasks.

Table 7. Ablation experiments. We train and test models on the DPDD dataset. For the baseline, we apply Restormer[68], a Transformer architecture based on channel attention(MDTA). T : the iteration numbers in the diffusion model

Network	Component	Params (M)	MACs (G)	PSNR (dB)
Baseline a	Transformer(MDTA)	25.05	1.93	26.66
Transformer block b	Transformer(Swin)	25.18	2.20	26.71
	Transformer(Swin+MDTA)	25.18	2.20	26.74
Pre-processing inference c	window size(256)+shift size(220)+Transformer(Swin+MDTA)	25.18	2.20	26.84
	window size(512)+shift size(220)+Transformer(Swin+MDTA)	25.18	2.20	26.98
	window size(512)+shift size(220)+Transformer(MDTA)	26.13	18.70	26.91
	window size(512)+shift size(384)+Transformer(Swin+MDTA)	25.18	2.20	26.89
Diffusion prior d	T(5)+Transformer(MDTA)	138.8	8.02	26.67
	T(10)+Transformer(MDTA)	138.8	8.02	26.71
	T(20)+Transformer(MDTA)	138.8	8.02	26.75
	T(50)+Transformer(MDTA)	138.8	8.02	26.77
Overall	T(50)+window size(512)+shift size(220)+Transformer(Swin +MDTA)	154.89	8.02	27.07

References

- [1] A. Abuolaim and M. Brown. Defocus deblurring using dual-pixel data. In *European Conference on Computer Vision (ECCV)*, 2020.
- [2] A. Abuolaim, M. Delbracio, D. Kelly, M. S. Brown, and P. Milanfar. Learning to reduce defocus blur by realistically modeling dual-pixel data. In *ICCV*, 2021.
- [3] I. Beltagy, M. E. Peters, and A. Cohan. Longformer: The Long-Document Transformer. *arXiv e-prints*, 2020.
- [4] H. C. Burger, C. J. Schuler, and S. Harmeling. Image denoising: Can plain neural networks compete with BM3D? In *CVPR*, 2012.
- [5] L. Chen, X. Chu, X. Zhang, and J. Sun. Simple baselines for image restoration. *arXiv preprint arXiv:2204.04676*, 2022.
- [6] L. Chen, X. Lu, J. Zhang, X. Chu, and C. Chen. Hinet: Half instance normalization network for image restoration. In *Proceedings of the IEEE/CVF Conference on Computer Vision and Pattern Recognition*, pages 182–192, 2021.
- [7] X. Chen, X. Wang, W. Zhang, X. Kong, Y. Qiao, J. Zhou, and C. Dong. Hat: Hybrid attention transformer for image restoration. *arXiv preprint arXiv:2309.05239*, 2023.
- [8] W. Cheng, M. Zhao, Z. Ye, and S. Gu. Mfagan: A compression framework for memory-efficient on-device super-resolution gan. *arXiv preprint arXiv:2107.12679*, 2021.
- [9] R. Child, S. Gray, A. Radford, and I. Sutskever. Generating Long Sequences with Sparse Transformers. *CoRR*, abs/1904.10509, 2019.
- [10] S.-J. Cho, S.-W. Ji, J.-P. Hong, S.-W. Jung, and S.-J. Ko. Rethinking coarse-to-fine approach in single image deblurring. In *Proceedings of the IEEE/CVF International Conference on Computer Vision*, pages 4641–4650, 2021.
- [11] K. M. Choromanski, V. Likhoshervstov, D. Dohan, X. Song, A. Gane, T. Sarlos, and et al. Rethinking Attention with Performers. In *ICLR*, 2021.
- [12] X. Chu, L. Chen, C. Chen, and X. Lu. Improving image restoration by revisiting global information aggregation. *arXiv preprint arXiv:2112.04491*, 2021.
- [13] X. Chu, L. Chen, C. Chen, and X. Lu. Improving image restoration by revisiting global information aggregation. *arXiv preprint arXiv:2112.04491*, 2021.
- [14] Y. N. Dauphin, A. Fan, M. Auli, and D. Grangier. Language modeling with gated convolutional networks. In *ICML*, 2017.
- [15] X. Deng, Y. Zhang, M. Xu, S. Gu, and Y. Duan. Deep coupled feedback network for joint exposure fusion and image super-resolution. *IEEE Transactions on Image Processing*, 30:3098–3112, 2021.
- [16] P. Dhariwal and A. Nichol. Diffusion models beat GANs on image synthesis. *CoRR*, abs/2105.05233, 2021.
- [17] A. Dosovitskiy, L. Beyer, A. Kolesnikov, D. Weissenborn, X. Zhai, T. Unterthiner, M. Dehghani, M. Minderer, G. Heigold, S. Gelly, et al. An image is worth 16x16 words: Transformers for image recognition at scale. In *ICLR*, 2021.
- [18] P. Esser, R. Rombach, and B. Ommer. Taming transformers for high-resolution image synthesis, 2020.
- [19] X. Fu, M. Wang, X. Cao, X. Ding, and Z.-J. Zha. A model-driven deep unfolding method for jpeg artifacts removal. *IEEE Transactions on Neural Networks and Learning Systems*, 2021.
- [20] X. Fu, Z.-J. Zha, F. Wu, X. Ding, and J. Paisley. Jpeg artifacts reduction via deep convolutional sparse coding. In *IEEE International Conference on Computer Vision*, pages 2501–2510, 2019.
- [21] M. Ghahremani, M. Khateri, A. Sierra, and J. Tohka. Adversarial distortion learning for medical image denoising. *arXiv:2204.14100*, 2022.
- [22] Y. Guo, J. Chen, J. Wang, Q. Chen, J. Cao, Z. Deng, Y. Xu, and M. Tan. Closed-loop matters: Dual regression networks for single image super-resolution. In *IEEE Conference on Computer Vision and Pattern Recognition*, pages 5407–5416, 2020.
- [23] J. Ho, A. Jain, and P. Abbeel. Denoising diffusion probabilistic models. In *NeurIPS*, 2020.
- [24] P. Isola, J.-Y. Zhu, T. Zhou, and A. A. Efros. Image-to-image translation with conditional adversarial networks. In *2017 IEEE Conference on Computer Vision and Pattern Recognition (CVPR)*, pages 5967–5976, 2017.
- [25] A. Karaali and C. R. Jung. Edge-based defocus blur estimation with adaptive scale selection. *TIP*, 2017.
- [26] T. Karras, S. Laine, M. Aittala, J. Hellsten, J. Lehtinen, and T. Aila. Analyzing and improving the image quality of StyleGAN. In *Proc. CVPR*, 2020.
- [27] A. Katharopoulos, A. Vyas, N. Pappas, and F. Fleuret. Transformers are RNNs: Fast Autoregressive Transformers with Linear Attention. In *ICML*, volume 119, pages 5156–5165, 2020.

- [28] Y. Kim, J. W. Soh, J. Park, B. Ahn, H.-S. Lee, Y.-S. Moon, and N. I. Cho. A pseudo-blind convolutional neural network for the reduction of compression artifacts. *IEEE Transactions on Circuits and Systems for Video Technology*, 30(4):1121–1135, 2019.
- [29] D. P. Kingma and M. Welling. Auto-encoding variational Bayes. *arXiv preprint arXiv:1312.6114*, 2013.
- [30] N. Kitaev, L. Kaiser, and A. Levskaya. Reformer: The Efficient Transformer. In *ICLR*, 2020.
- [31] J. Lee, S. Lee, S. Cho, and S. Lee. Deep defocus map estimation using domain adaptation. In *CVPR*, 2019.
- [32] J. Lee, H. Son, J. Rim, S. Cho, and S. Lee. Iterative filter adaptive network for single image defocus deblurring. In *Proceedings of the IEEE/CVF Conference on Computer Vision and Pattern Recognition*, pages 2034–2042, June 2021.
- [33] J. Li, A. Hassani, S. Walton, and H. Shi. Convmlp: Hierarchical convolutional mlps for vision, 2021.
- [34] J. Liang, J. Cao, G. Sun, K. Zhang, L. Van Gool, and R. Timofte. SwinIR: Image restoration using swin transformer. In *ICCV Workshops*, 2021.
- [35] J. Liang, J. Cao, G. Sun, K. Zhang, L. Van Gool, and R. Timofte. SwinIR: Image restoration using swin transformer. In *IEEE Conference on International Conference on Computer Vision Workshops*, 2021.
- [36] J. Liang, A. Lugmayr, K. Zhang, M. Danelljan, L. Van Gool, and R. Timofte. Hierarchical conditional flow: A unified framework for image super-resolution and image rescaling. In *IEEE Conference on International Conference on Computer Vision*, 2021.
- [37] J. Liang, G. Sun, K. Zhang, L. Van Gool, and R. Timofte. Mutual affine network for spatially variant kernel estimation in blind image super-resolution. In *IEEE Conference on International Conference on Computer Vision*, 2021.
- [38] J. Liang, K. Zhang, S. Gu, L. Van Gool, and R. Timofte. Flow-based kernel prior with application to blind super-resolution. In *IEEE Conference on Computer Vision and Pattern Recognition*, pages 10601–10610, 2021.
- [39] H. Liu, Z. Dai, D. R. So, and Q. V. Le. Pay attention to mlps, 2021.
- [40] Z. Liu, Y. Lin, Y. Cao, H. Hu, Y. Wei, Z. Zhang, S. Lin, and B. Guo. Swin transformer: Hierarchical vision transformer using shifted windows. In *Proceedings of the IEEE/CVF International Conference on Computer Vision (ICCV)*, 2021.
- [41] I. Loshchilov and F. Hutter. SGDR: Stochastic gradient descent with warm restarts. In *ICLR*, 2017.
- [42] Z. Luo, F. K. Gustafsson, Z. Zhao, J. Sjölund, and T. B. Schön. Image restoration with mean-reverting stochastic differential equations, 2023.
- [43] X. Mao, Y. Liu, W. Shen, Q. Li, and Y. Wang. Deep residual fourier transformation for single image deblurring. *arXiv preprint arXiv:2111.11745*, 2021.
- [44] S. Nah, T. Hyun Kim, and K. Mu Lee. Deep multi-scale convolutional neural network for dynamic scene deblurring. In *Proceedings of the IEEE conference on computer vision and pattern recognition*, pages 3883–3891, 2017.
- [45] T. Park, M.-Y. Liu, T.-C. Wang, and J.-Y. Zhu. Semantic image synthesis with spatially-adaptive normalization. In *Proceedings of the IEEE/CVF Conference on Computer Vision and Pattern Recognition (CVPR)*, June 2019.
- [46] W. Peebles and S. Xie. Scalable diffusion models with transformers, 2023.
- [47] S. E. Reed, Z. Akata, X. Yan, L. Logeswaran, B. Schiele, and H. Lee. Generative adversarial text to image synthesis. In *ICML*, 2016.
- [48] R. Rombach, A. Blattmann, D. Lorenz, P. Esser, and B. Ommer. High-resolution image synthesis with latent diffusion models, 2021.
- [49] O. Ronneberger, P. Fischer, and T. Brox. U-net: Convolutional networks for biomedical image segmentation. In *MICCAI (3)*, volume 9351 of *Lecture Notes in Computer Science*, pages 234–241. Springer, 2015.
- [50] O. Ronneberger, P. Fischer, and T. Brox. U-Net: convolutional networks for biomedical image segmentation. In *MICCAI*, 2015.
- [51] J. Shi, L. Xu, and J. Jia. Just noticeable defocus blur detection and estimation. In *CVPR*, 2015.
- [52] W. Shi, J. Caballero, F. Huszár, J. Totz, A. P. Aitken, R. Bishop, D. Rueckert, and Z. Wang. Real-time single image and video super-resolution using an efficient sub-pixel convolutional neural network. In *CVPR*, 2016.
- [53] K. Simonyan and A. Zisserman. Very deep convolutional networks for large-scale image recognition. *arXiv preprint arXiv:1409.1556*, 2014.
- [54] H. Son, J. Lee, S. Cho, and S. Lee. Single image defocus deblurring using kernel-sharing parallel atrous convolutions. In *ICCV*, 2021.
- [55] Y. Song, J. Sohl-Dickstein, D. P. Kingma, A. Kumar, S. Ermon, and B. Poole. Score-based generative modeling through stochastic differential equations. *CoRR*, abs/2011.13456, 2020.
- [56] Y. Tay, D. Bahri, D. Metzler, D.-C. Juan, Z. Zhao, and C. Zheng. Synthesizer: Rethinking Self-Attention in Transformer Models. *arXiv e-prints*, 2020.
- [57] Y. Tay, D. Bahri, L. Yang, D. Metzler, and D.-C. Juan. Sparse Sinkhorn Attention. In *ICML*, volume 119, pages 9438–9447, 2020.
- [58] Y. Tay, M. Dehghani, S. Abnar, Y. Shen, D. Bahri, P. Pham, and et al. Long Range Arena: A Benchmark for Efficient Transformers. In *ICLR*, 2021.
- [59] Z. Tu, H. Talebi, H. Zhang, F. Yang, P. Milanfar, A. Bovik, and Y. Li. Maxim: Multi-axis mlp for image processing. *arXiv preprint arXiv:2201.02973*, 2022.
- [60] A. Vaswani, N. Shazeer, N. Parmar, J. Uszkoreit, L. Jones, A. N. Gomez, L. Kaiser, and I. Polosukhin. Attention is all you need. In *Proceedings of NeurIPS*, pages 5998–6008, 2017.
- [61] L. Wang, Y. Wang, Z. Lin, J. Yang, W. An, and Y. Guo. Learning a single network for scale-arbitrary super-resolution. In *IEEE Conference on International Conference on Computer Vision*, pages 10581–10590, 2021.
- [62] S. Wang, B. Z. Li, M. Khabsa, H. Fang, and H. Ma. Linformer: Self-Attention with Linear Complexity. *arXiv e-prints*, 2020.

- [63] X. Wang, R. Girshick, A. Gupta, and K. He. Non-local neural networks. In *CVPR*, 2018.
- [64] Z. Wang, X. Cun, J. Bao, and J. Liu. Uformer: A general u-shaped transformer for image restoration. *arXiv preprint arXiv:2106.03106*, 2021.
- [65] Yawei Li, Yuchen Fan, Xiaoyu Xiang, Denis Demandolx, Rakesh Ranjan, Radu Timofte, and Luc Van Gool. Efficient and explicit modelling of image hierarchies for image restoration. In *Proceedings of the IEEE Conference on Computer Vision and Pattern Recognition*, 2023.
- [66] W. Yu, M. Luo, P. Zhou, C. Si, Y. Zhou, X. Wang, J. Feng, and S. Yan. Metaformer is actually what you need for vision. In *Proceedings of the IEEE/CVF Conference on Computer Vision and Pattern Recognition*, pages 10819–10829, 2022.
- [67] M. Zaheer, G. Guruganesh, K. A. Dubey, J. Ainslie, C. Alberti, S. Ontanon, and et al. Big Bird: Transformers for Longer Sequences. In *NeurIPS*, volume 33, pages 17283–17297, 2020.
- [68] S. W. Zamir, A. Arora, S. Khan, M. Hayat, F. S. Khan, and M.-H. Yang. Restormer: Efficient transformer for high-resolution image restoration. In *CVPR*, 2022.
- [69] H. Zhang, I. Goodfellow, D. Metaxas, and A. Odena. Self-attention generative adversarial networks. In *ICML*, 2019.
- [70] Y. Zhang, D. Li, X. Shi, D. He, K. Song, X. Wang, H. Qin, and H. Li. Kbnnet: Kernel basis network for image restoration. *arXiv preprint arXiv:2303.02881*, 2023.